EFFECTIVE STRESS IN UNSATURATED GRANULAR MATERIALS: MICRO-MECHANICAL INSIGHTS

JÉRÔME DURIEZ[*], RICHARD WAN[*]

[*]Departement of Civil Engineering
University of Calgary
Calgary, AB, T2B 1N4, Canada
e-mail: jerome.duriez@ucalgary.ca

Key words: Unsaturated material, Pendular regime, Micro-mechanics, Effective stress, Discrete Element Method

Abstract. Stress transport in an unsaturated granular material is analytically derived. As such, an effective stress tensor related to the mechanical state governed by the interganular forces within the skeleton is identified together with a capillary stress tensor that accounts for the interactions due to the liquid and gaseous phases. Using a Discrete Element Method for modelling an unsaturated granular material, this capillary stress tensor is computed along different loading paths. Knowing the applied total stress, the effective stress tensor is then readily deduced and it is shown that it describes adequately the strength of the unsaturated granular material along various loading paths for any degree of saturation.

1 INTRODUCTION

Geomaterials encountered in Civil Engineering are multiphasic systems which typically encompass solid, liquid (wetting) and gas (non-wetting) phases. Considering granular geomaterials, the solid phase is discontinuous, consisting of a collection of distinct soil particles. Voids exist between the particles, and we denote the union of the solid phase and these voids as the skeleton. Most of the classical analyses of geomaterials pertain to limiting conditions represented by the void space containing only gas (dry case) or only liquid (saturated case). However, conditions encountered in geotechnical practice involve unsaturated soils, for which these voids include both liquid and gas phases. The presence of the three phases and their mutual interactions enrich their mechanical behaviour, leading for example, to higher strengths depending on the water content. As such, we tackle here this unsaturated case. Various filling configurations of the liquid phase within the void space exist depending on the degree of saturation S_r, *i.e.* the ratio between the water volume, and the volume of the voids. Here, a *pendular regime* is invoked where the

liquid phase consists of distinct menisci between soil particles (Figure 1), corresponding to low values of degree of saturation ($S_r < 20\%$).
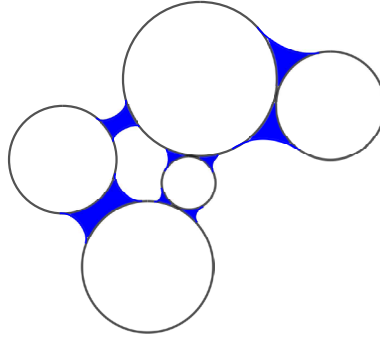

Figure 1: Unsaturated granular material in the pendular regime: water phase forms distinct menisci between contacting and some distant soil particles (idealized as spheres)

We aim here to analyze the mechanical state of unsaturated granular materials, and to investigate how it relates to skeleton behaviour. To this end, analytical derivations of stress transport in the unsaturated material are introduced in Section 2, identifying an *effective stress* related to the skeleton. Then, these newly derived analytical expressions are used in a DEM simulation of an unsaturated granular soil [1] to verify the role of effective stress in governing material strength.

2 FORCE TRANSPORT IN UNSATURATED MEDIA

2.1 Analytical derivations

In [2], the total, or macroscopic, stress for the volume V of unsaturated material depicted in Figure 1 has been computed as an average of the stresses existing in the different phases. The stresses inside the liquid or gaseous phases are readily computed as $\boldsymbol{\sigma} = u_\alpha \boldsymbol{\delta} \; \forall \vec{x} \in V_\alpha$, with V_α, $\alpha = l, g$, the volume of the phase α, u_α its uniform pressure, and $\boldsymbol{\delta}$ the identity tensor. Note that geomechanics sign convention is used troughout this paper, with compressive stresses and strains being positive.

The stress within the solid phase is computed from local stresses inside each particle, assuming they are in static equilibrium without body forces: $div(\boldsymbol{\sigma}) = \vec{0} \; \forall \vec{x} \in V_s^k$, with V_s^k the volume of the solid particle k. Under this assumption, the volume integrals of $\boldsymbol{\sigma}$ are classically computed from the external tractions existing on the boundaries on each particle. Taking into account the solid contact forces, as well as the loadings of the water pressure along all wetted surfaces S_l^k, of the air pressure along all dry surfaces S_g^k, and of the surface tension along all menisci contours Γ_m^k (*i.e.* the intersection of solid, liquid, and gaseous phases along the particle k), the total stress is finally obtained as:

$$\boldsymbol{\sigma} = \frac{1}{V} \sum_{cont.\,s-s} \vec{f} \otimes \vec{l} + u_g\,\boldsymbol{\delta} - (u_g - u_l)\boldsymbol{\chi} - \boldsymbol{B} \tag{1}$$

$$\boldsymbol{\chi} = \frac{V_l}{V}\boldsymbol{\delta} + \frac{1}{V}\sum_k \int_{S_l^k} R^k \vec{n} \otimes \vec{n}\,dS$$

$$\boldsymbol{B} = \frac{1}{V}\sum_k \int_{\Gamma_m^k} \vec{\gamma} \otimes R^k \vec{n}\,dl$$

In equation (1), the vectors $\vec{f}$ and $\vec{l}$ are defined for each contact between two solid grains "1" and "2": $\vec{f}$ is the contact force, as acting on the grain 2, and $\vec{l}$ is the branch vector joining the two particles centers, from 1 to 2. The R^k are the radii of the solid particles considered as spherical whereas $\vec{\gamma}\,dl$ is the incremental surface tension acting on one particle k, at one point of a meniscus contour along this particle.

This analytical model is currently being extended to take into account the interfaces between the different phases, these interfaces having their own energies and stresses [3, 4].

2.2 Discussion

In equation (1), the first term in the expression of $\boldsymbol{\sigma}$ corresponds to the Love-Weber formula [5, 6]. It is related to the skeleton behaviour, as it will be shown in Section 3. Thus, it is denoted as *effective stress*.

In addition to this effective stress, two other stress-like tensors arise from the derivations, neglecting the air pressure $u_g\,\boldsymbol{\delta}$. They correspond to the mechanical interactions due to the presence of both liquid and gaseous phases. For this reason, their sum is denoted as *capillary stress*.

One term of the capillary stress is proportionnal to the matric suction $u_g - u_l$, with a symmetric tensor $\boldsymbol{\chi}$ depending on the distribution of the water phase around the solid particles. This tensor is isotropic, *i.e.* spherical, if and only the above-mentioned distribution is isotropic. The water phase distribution being to a certain extent controlled by the distribution of grain contacts, a deviatoric nature for $\boldsymbol{\chi}$ may arise during a deviatoric loading, due to induced anisotropy [7].

A second term, denoted $\boldsymbol{B}$, describes the mechanical action on the solid grains of the surface tension existing at the liquid-gas interface. In case of a monosized granular material, with an isotropic distribution of liquid phase, this tensor vanishes [2]. In other cases, this tensor is a non-null deviatoric one since, assuming a null contact angle:

$$tr(\boldsymbol{B}) = \frac{1}{V}\sum_k \int_{\Gamma_m^k} R^k \vec{n}.\vec{\gamma_{lg}}\,d\Gamma = 0 \tag{2}$$

According to equation (1), the sum of these two terms, $(u_g - u_l)\boldsymbol{\chi} + \boldsymbol{B}$, is equal to the difference between the effective stress $1/V \sum \vec{f} \otimes \vec{l}$ and the total one $\boldsymbol{\sigma}$. Conversely,

for a known distribution of the water phase in an unsaturated granular material under a total stress $\boldsymbol{\sigma}$, equation (1) can be applied to determine the effective stress related to the granular skeleton: $\boldsymbol{\sigma} + (u_g - u_l)\boldsymbol{\chi} + \boldsymbol{B}$. Note that for the saturated case, equation (1) reduces to Terzaghi's equation.

3 COMPARISON WITH DISCRETE SIMULATIONS

3.1 The DEM model

Simulations of an unsaturated granular material are performed using the code Yade [8], that is based on the Discrete Element Method [9]: the model describes the mechanical state of a collection of discrete elements that correspond to the soil particles. In addition to the contact forces between touching elements, the model includes capillary forces acting on elements. Introducing these capillary forces allows us to simulate the liquid bridges (menisci) of the pendular regime [1].

The contact between particles is governed by frictional elastic-plastic contact laws. Repulsive normal forces act when spheres get closer and they are linearly computed from the relative normal displacement. Contact forces include tangential forces too, computed linearly from the relative tangential displacement up to a plastic threshold obeying Coulomb friction law. This part of the model depends on three micro-parameters: two local stiffnesses, and one microscopic (inter-particle) friction angle. Values used in [1] are retained.

Suction controlled simulations are performed based on an algorithm solving the Laplace equation that describes pendular menisci [1]. From the surface tension, the suction $u_g - u_l$, and features of the numerical packing (radii and distance between elements), a distribution of menisci results directly from the algorithm. Menisci characteristic features are then derived, such as filling angles, volumes, and associated forces acting on grains. Assuming a wetting loading path (increasing S_r), menisci are created between touching particles, and exist between these particles as long as a solution is found for Laplace equation. In particular, menisci still exist when the particles do not touch anymore, leading to distant attractive forces.

Different loading paths may be simulated, using periodic and non-periodic boundary conditions. Periodic and non-periodic triaxial paths ($\sigma_I = \sigma_{yy} > \sigma_{II} = \sigma_{xx} = \sigma_{III} = \sigma_{zz} = cst$) are considered, as well as periodic simple shear tests ($\partial v_x / \partial y = cst$, $\sigma_{yy} = \sigma_{zz} = cst$), see Figure 2. Periodic simulations rely on the homogeneous strain of an unit cell including the sample (see [10] for details). Non-periodic simulations involve rigid frictionless boundaries whose movements impose strain onto the numerical sample.

Periodic and non-periodic simulations were performed on two similar numerical samples. The two samples, one periodic and another non-periodic, include 20,000 spherical particles obeying an uniform size distribution with $D_{max}/D_{min} = 3$ and $D_{50} = 45.3 \pm 0.5\,\mu m$. The porosity of the two samples under 1 kPa isotropic pressure is 0.36 ± 0.01, leading to a dilatant behaviour for confining pressures in the range [1; 20 kPa].
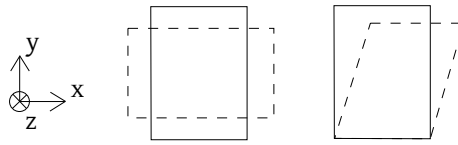
Figure 2: Triaxial (axisymmetric) compression: left, and simple shear: right

3.2 Discrete results for the dry case

The failure of the granular material is first investigated in the dry case, without introducing any capillary forces in the model. Limit stress states for the two samples along various loading paths are depicted in Figure 3 according to the first and second invariants of $\boldsymbol{\sigma}$: the mean stress $p = (\sigma_I + \sigma_{II} + \sigma_{III})/3$ and the deviatoric stress $q = \sqrt{3/2} * ||\boldsymbol{\sigma} - p\,\mathbf{1}||$ ($q = \sigma_I - \sigma_{III}$ for the triaxial paths). Since the plastic limit criterion of granular materials also depends on the third invariant, deviatoric stresses for simple shear paths are corrected according to the current Lode angle, θ, values, assuming a Lade criterion [11]. As such, direct comparison is possible between the various loading paths, despite different θ values ($\theta = 0°$ for triaxial compression, while, here, $\theta \in [22°; 30°]$ for simple shear). As is evidenced in Figure 3, all stress limit states obey a common Mohr-Coulomb (MC) criterion, with a macroscopic friction angle $\phi = 29°$.
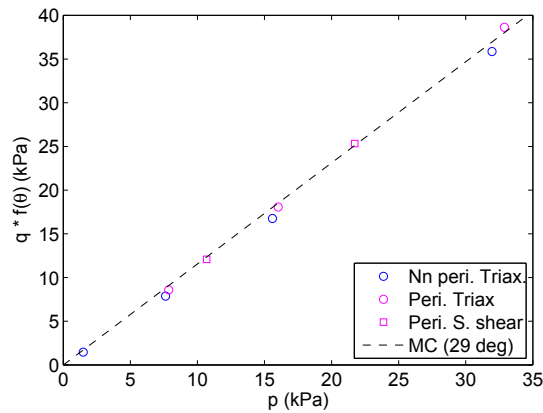

Figure 3: Stress limit states according to the mean and deviatoric stresses, p and q. Deviatoric stresses for simple shear tests are corrected to be directly compared to values of triaxial tests, despite the difference in Lode angle θ

3.3 Discrete results for the unsaturated case

The model is then applied to the unsaturated conditions. Six non-periodic triaxial loadings are simulated for different confining pressures, in {5;10} kPa, and suction values, in {10;50;100;300} kPa, see Table 1. Associated degrees of saturation values are low (below 10%) ensuring a pendular regime.

Table 1: Initial degrees of saturation (%) for the simulated unsaturated triaxial loadings

		$u_g - u_l$ (kPa)			
		10	50	100	300
σ_{xx} (kPa)	5	-	-	0.32	0.045
	10	8.7	1.0	0.32	0.046

Classically, limit stress states in unsaturated conditions correspond to higher deviatoric stresses, not obeying anymore to the Mohr-Coulomb determined from the dry case (Figure 4).
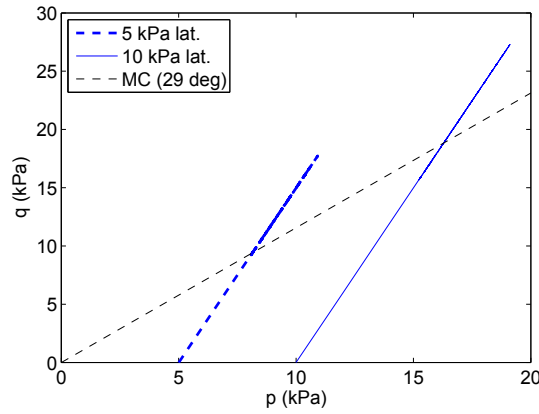

Figure 4: Stress paths for two unsaturated triaxial loadings with 100 kPa suction, and different lateral pressures

Indeed, due to the presence of liquid and gaseous phases, the effective stresses related to the solid phase are now different from the total stresses (Figure 5). All stress tensors being axisymmetric around $\vec{y}$ axis (see Figure 2) during triaxial loadings, it is sufficient to consider the mean (one third of the trace) and deviatoric ($yy - xx$) components of each tensor. Both water and gaseous phases induce mainly a change in mean stresses. The deviatoric component of the capillary stress tensor is here small, so that there is not much of a difference between deviatoric effective and total stresses. This is related to the initial isotropy of the DEM packing (see [2] for a study of inherent anisotropic packings), which is consistent with initial null values of the deviatoric stress. However, because of the induced anisotropy at the solid contact scale, a deviatoric feature for the capillary stress tensor is induced by the loading (see also the Figures 7 and 8) and this deviatoric feature increases with suction (Figure 6).

Among the two terms forming the capillary stress tensor, $(u_g - u_l)\boldsymbol{\chi}$ is rather predominant with respect to $\boldsymbol{B}$ (compare Figures 7 and 8). However, the relative magnitudes of these two terms depend on the suction. Indeed, the deviatoric component of $(u_g - u_l)\boldsymbol{\chi}$
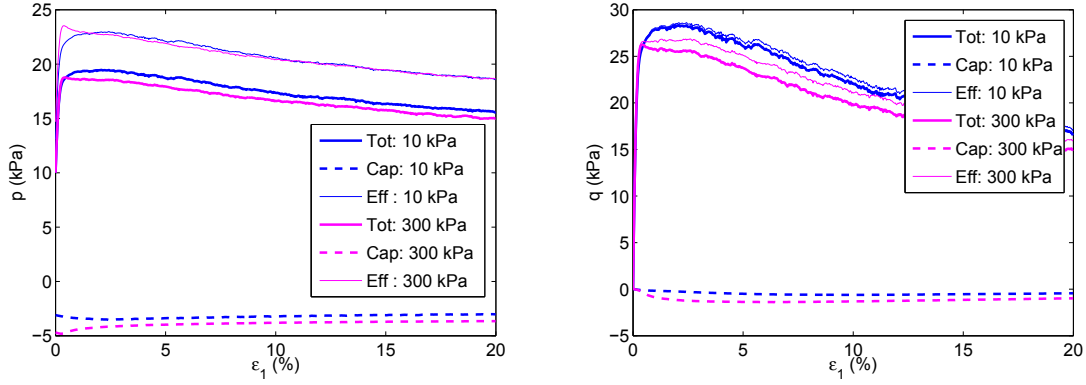
Figure 5: Mean (left) and deviatoric (right) components of the different stress tensors during two unsaturated triaxial loadings, under 10 kPa lateral pressure, and two different suctions. Capillary stress tensor is $(u_g - u_l)\boldsymbol{\chi} + \boldsymbol{B}$, and effective stress tensor is $\boldsymbol{\sigma} - (u_g - u_l)\boldsymbol{\chi} - \boldsymbol{B}$
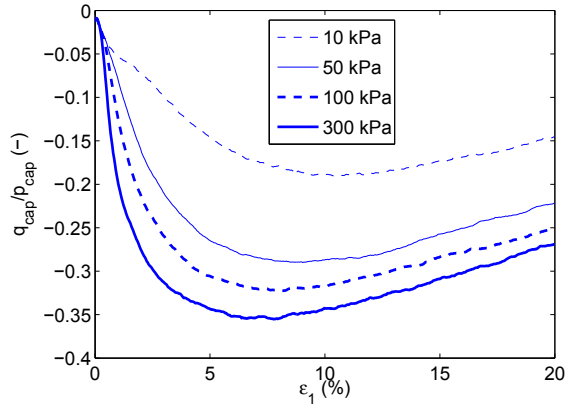

Figure 6: Deviatoric feature of the capillary stress tensor $(u_g - u_l)\boldsymbol{\chi} + \boldsymbol{B}$ for triaxial loadings under 10 kPa lateral pressure and different suctions

increases considerably from initial small values with suction (Figure 7) whereas on the other hand the deviatoric component of $\boldsymbol{B}$ (*i.e.* its norm) decreases significantly from large values with suction (Figure 8). This is because, for increasing suction, both degree of saturation and filling angles decrease in the granular material, leading to lower menisci contour, and lower values for the components of $\boldsymbol{B}$. In the end, for high suction values, $(u_g - u_l)\boldsymbol{\chi}$ is the main contributor to the capillary deviatoric stresses. On the other hand, for low suctions, deviatoric capillary stresses arise mainly thanks to $\boldsymbol{B}$.

Periodic unsaturated simple shear simulations, with $\sigma_{xx} = \sigma_{yy} = 10$ kPa, are also performed for different suction values. Corresponding degrees of saturation (for the initial states) are detailed in Table 2. The same trends concerning the relative magnitudes of these two terms are observed during simple shear than triaxial conditions (Figures 9 and 10).
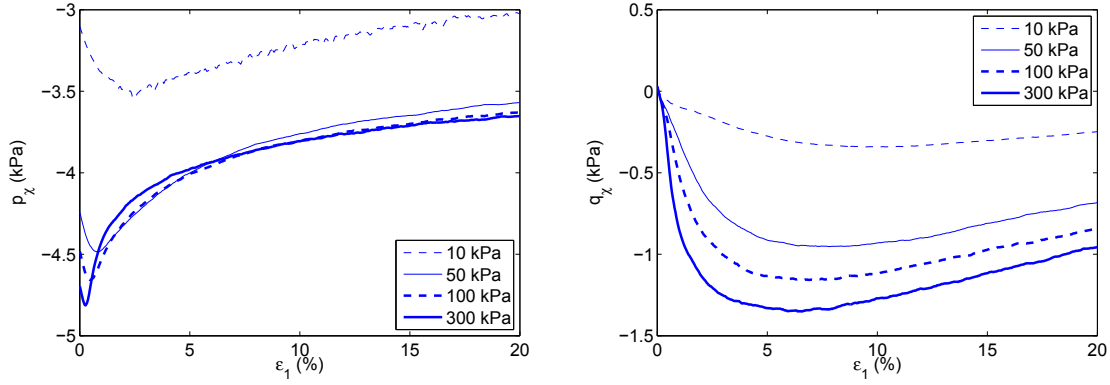
Figure 7: Mean (left) and deviatoric (right) components of $(u_g - u_l)\boldsymbol{\chi}$ for triaxial loadings under 10 kPa lateral pressure and different suctions
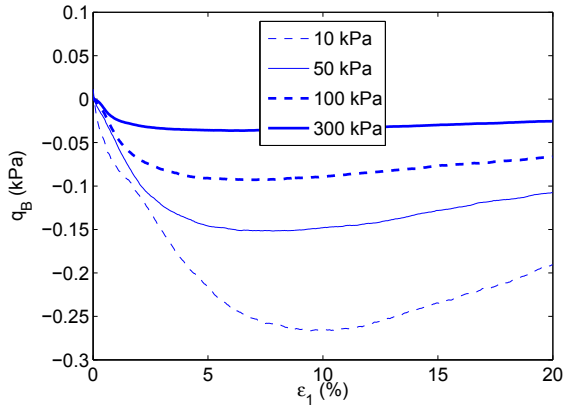

Figure 8: Deviatoric component of $\boldsymbol{B}$ for triaxial loadings under 10 kPa lateral pressure and different suctions (remind that $tr(\boldsymbol{B}) = 0$)

Table 2: Initial saturation ratios (%) for the unsaturated simple shears

$u_g - u_l$ (kPa)			
10	50	100	300
10.1	1.2	0.37	0.054

3.4 A comprehensive plastic limit criterion for dry and unsaturated cases

For the various loading paths simulated in unsaturated conditions, effective stresses $\boldsymbol{\sigma'}$ related to the skeleton are deduced from the total and capillary stresses. Note that the DEM model offers a direct computation of effective stresses [1], which is not done here. As in the previous Section 3.2, limit stress states are determined and plotted in the (p', q')
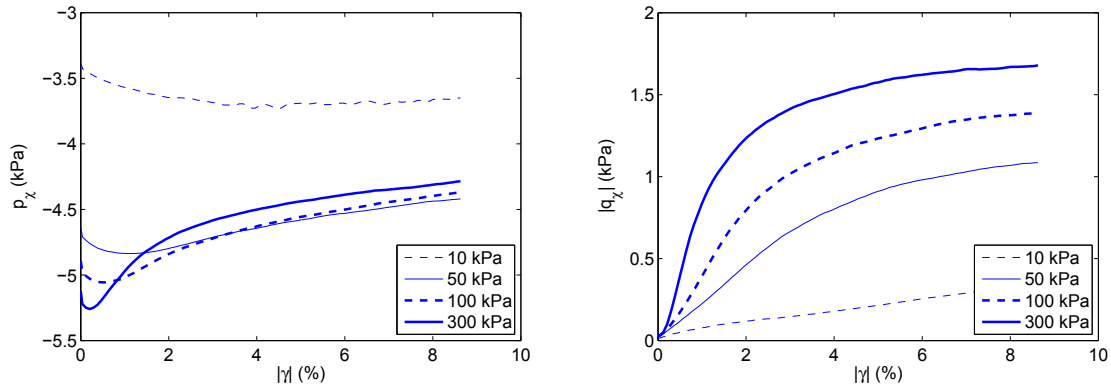
Figure 9: Mean (left) and deviatoric (right) components of $(u_g - u_l)\boldsymbol{\chi}$ for simple shear loadings with different suctions
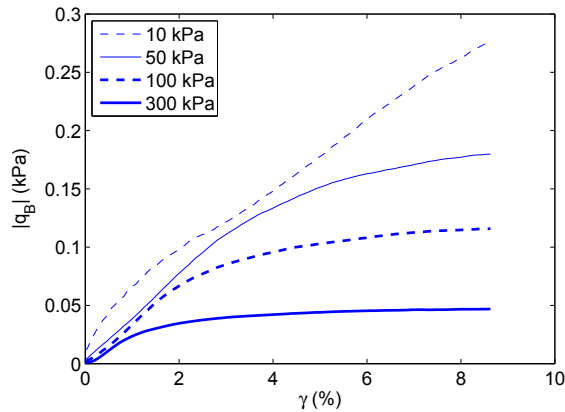

Figure 10: Deviatoric component of $\boldsymbol{B}$ for simple shear loadings with different suctions

plane (Figure 11). The Mohr-Coulomb criterion determined from the dry case in Section 3.2 is obeyed with an acceptable dispersion. This validates the relevancy of the effective stress derived in equation (1) to express the strength of a granular material, whatever its saturation ratio.

4 Conclusion

Analytical derivations of stress transport in an unsaturated granular media identified an effective stress related to the mechanical state governed by intergranular forces within skeleton, and a capillary stress arising from the mechanical interactions due to the liquid and gaseous phases. This capillary stress depends on the packing and on the liquid phase distribution inside the material. This stress is non-spherical for anisotropic liquid distribution, as it has been evidenced in case of loading-induced anisotropy. This deviatoric feature of the capillary stress increases with matric suction.
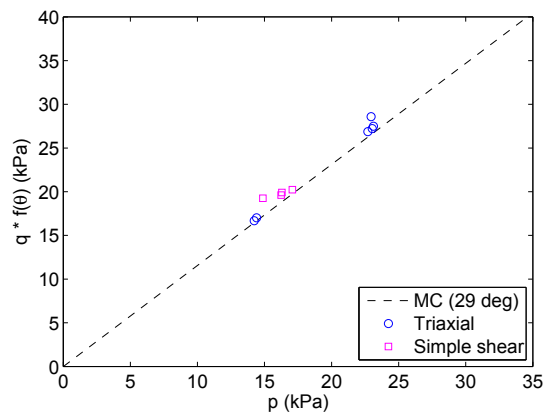
Figure 11: Limit stress states for unsaturated cases along different loading paths, compared with the dry Mohr-Coulomb criterion deduced from the dry case

In fact, two tensorial terms accounting for the capillary actions can be distinguished, with one deviatoric in case of a null contact angle. Relative magnitudes of these two terms depend on the suction.

Determining such capillary stress allows us to identify the effective stress tensor. It is shown that this effective stress tensor is an adequate variable to express the strength of an unsaturated granular material, along various loading paths irrespective of the degree of saturation.

REFERENCES

[1] L. Scholtès, B. Chareyre, F. Nicot, and F. Darve. Micromechanics of granular materials with capillary effects. *International Journal of Engineering Science*, 47(1):64 – 75, 2009.

[2] R. Wan, S. Khosravani, and M. Pouragha. Micromechanical analysis of force transport in wet granular soils. *Vadose Zone Journal*, 13(5):1–12, 2014.

[3] Norman R. Morrow. Physics and thermodynamics of capillary action in porous media. *Industrial & Engineering Chemistry*, 62(6):32–56, 1970.

[4] Xavier Chateau and Luc Dormieux. Micromechanics of saturated and unsaturated porous media. *International Journal for Numerical and Analytical Methods in Geomechanics*, 26(8):831–844, 2002.

[5] A.E.H. Love. *A treatise on the mathematical theory of elasticity*. Cambridge University Press, Cambridge, 1927.

[6] J. Weber. Recherches concernant les contraintes intergranulaires dans les milieux pulvérulents. *Bulletin de liaison des Ponts et Chaussées*, 20:1–20, 1966.

[7] Masanobu Oda, Siavouche Nemat-Nasser, and Junichi Konishi. Stress-induced anisotropy in granular masses. *Soils and Foundations*, 25(3):85–97, 1985.

[8] V. Smilauer, E. Catalano, B. Chareyre, S. Dorofeenko, J. Duriez, A. Gladky, J. Kozicki, C. Modenese, L. Scholtès, L. Sibille, J. Stránský, and K. Thoeni. *Yade Documentation*. The Yade Project, 1st edition, 2010. http://yade-dem.org/doc/.

[9] P.A. Cundall and O.D.L. Strack. A discrete numerical model for granular assemblies. *Géotechnique*, 29:47–65, 1979.

[10] F. Radjai and C. Voivret. Periodic boundary conditions. In F. Radjai and F. Dubois, editors, *Discrete-element Modeling of Granular Materials*. ISTE-Wiley, 2011.

[11] Poul V. Lade and James M. Duncan. Elasto-plastic stress-strain theory for cohesionless soil. *Journal of the Geotechnical Engineering Division*, 101(10):1037–1053, 1975.